PNAS
www.pnas.org

Supplementary Information for

Structural basis for cooperative regulation of KIX-mediated transcription pathways by the HTLV-1 HBZ activation domain

Ke Yang, Robyn L. Stanfield, Maria A. Martinez-Yamout, H. Jane Dyson, Ian A. Wilson and Peter E. Wright

Corresponding Author: Peter E. Wright
Email: wright@scripps.edu

This PDF file includes:

Supplementary text
Figs. S1 to S9
Table S1
References for SI reference citations

www.pnas.org/cgi/doi/10.1073/pnas.1810397115

Supplementary Information Text
Materials and Methods

Protein Preparation. Three constructs of the HTLV-1 HBZ activation domain (HBZ AD, residues 3-56 and 3-77; HBZ AD1, residues 3-36) were expressed in *E. coli* as His_6-tagged GB1 fusion proteins. HBZ AD2 (residues 33-56) was expressed in *E. coli* as a His_6-SUMO fusion protein, with an extra serine residue at the N-terminus. All of the HBZ AD proteins were co-expressed with the KIX domain of CBP in order to reduce toxicity to *E. coli*. Cell pellets were resuspended in buffer A (8M urea, 600mM NaCl, 20mM Tris pH 8) and lysed by sonication. The fusion proteins were purified with Roche cOmplete His-Tag purification resin, eluted with elution buffer (600mM NaCl, 200mM imidazole, 20mM Tris pH 8) and dialyzed against dialysis buffer (100mM NaCl, 10mM Tris pH 8, 2mM DTT). The His_6-GB1 and His_6-SUMO tags were cleaved using TEV protease or Ulp1 protease in dialysis buffer. The cleaved HBZ AD proteins were further purified using reverse-phase HPLC. With the exception of the AD2 peptide, the resulting HBZ AD proteins contain additional residues (GSHM) at the N-terminus. The KIX domain of mouse CBP (residues 586-683) was expressed and purified as previously described (1). A 32 residue peptide spanning the mouse c-Myb transactivation domain (Myb32, residues 284-315) was expressed in *E. coli* as a His_6-SUMO fusion protein. The His_6-SUMO tag was cleaved using Ulp1 protease and removed using Roche cOmplete His-Tag resin. The cleaved Myb32 peptide was purified using reverse-phase HPLC. Lyophilized proteins were resuspended, buffer-exchanged and concentrated in 50mM Tris (pH 6.8) and 50mM NaCl.

Crystallization and Structure Determination of HBZ AD:KIX:Myb Ternary Complexes. HBZ(3-77):KIX:Myb (13.6mg/mL) and HBZ(3-56):KIX:Myb (12.0mg/mL) were formed by mixing concentrated stock of HBZ AD proteins, KIX and Myb at a ratio of 1:1:1 in 50mM Tris (pH 6.8) and 50mM NaCl. Crystallization screens were set up using the sitting drop vapor diffusion method. Crystals for KIX:Myb:HBZ(3-77 and 3-56) complexes were obtained within 3-7 days, under conditions 20% PEG 3350 with 0.2 M $CaCl_2$, and 20% PEG 3350 with 0.2 M NaI, respectively. Crystals were cryoprotected with 30% (vol/vol) ethylene glycol and flash-cooled in liquid nitrogen. Diffraction data

were collected at Stanford Synchrotron Radiation Lightsource (SSRL) beamline 9-2 and processed with HKL-2000 (2). Molecular replacement was performed using Phaser (3) with KIX:c-Myb25 chains from the solution structure ensemble of KIX:c-Myb25:MLL (DeGuzman et al. (4), PDB ID 2AGH), where all 20 NMR structures were used as ensemble input. Rigid body refinement of the best solution from Phaser resulted in high R values (R=51, Rfree=56%) and very poor electron density. This model was modified with the morph_model routine in Phenix (5), where the map to model correlation increased from 0.33 to 0.57 over 6 cycles. The resulting map was of good quality and enabled us to build the model with Coot (6). Models were refined with phenix.refine (7) and REFMAC5 (8), and structural figures were rendered with PyMOL (9).

NMR Spectroscopy. ^{15}N-labeled and ^{13}C, ^{15}N-labeled proteins were prepared by growing *E.coli* cells in isotope enriched M9 minimal media containing 3 g/L $^{13}C_6$-D-glucose for ^{13}C labeling and 1 g $(^{15}NH_4)_2SO_4$ for ^{15}N labeling). NMR spectra were acquired at 28 °C in NMR buffer (50mM Tris pH 6.8, 50mM NaCl, 10% vol/vol D_2O) using Bruker 500-, 700-, 800- and 900-MHz spectrometers. NMR data were processed and analyzed using NMRPipe (10) and NMRView (11). Backbone resonances were assigned using standard 3D triple resonance spectra of 600 μM ^{13}C, ^{15}N-labeled HBZ(3-56) in NMR buffer. Backbone amide assignments of free HBZ AD2 (residues 33-56) were transferred from those of HBZ(3-56) by comparison of ^{1}H-^{15}N HSQC spectra.

Isothermal titration calorimetry. ITC measurements were performed using a MicroCal iTC200 instrument. Samples were dialyzed against 50mM Tris pH 6.8, 50mM NaCl prior to the measurements. KIX, or the pre-formed 1:1 KIX:c-Myb or KIX:HBZ complexes were placed in the cell at concentrations ranging from 5 to 80 μM. The HBZ or c-Myb peptides were loaded into the syringe at concentrations between 25 and 800 μM. The concentrations of KIX and c-Myb were determined from the absorbance at 280 nm using calculated extinction coefficients. Due to lack of UV absorbance at 280nm, the HBZ concentration was determined using standard curves calibrated using analytical reverse-phase HPLC with absorbance monitored at 214nm. Unless otherwise indicated, experiments were carried out in triplicate at 28 °C and consisted of at least 16 injections

with duration of 5s, spacing of 180s, and reference power at 5μCal. The data were processed with the Origin 7.0 software and fitted to a one-site binding model to derive K_d and ΔH values. ΔG and ΔS were calculated from standard thermodynamic equations, $\Delta G = RT\ln K_d$ and $\Delta G = \Delta H - T\Delta S$.

Circular dichroism (CD). CD spectra of HBZ AD constructs (3-77, 3-56, 3-36 and 33-56) in buffer containing 50mM Tris pH 6.8 and 50mM NaCl were measured at 28 °C on an Aviv62DS spectropolarimeter.

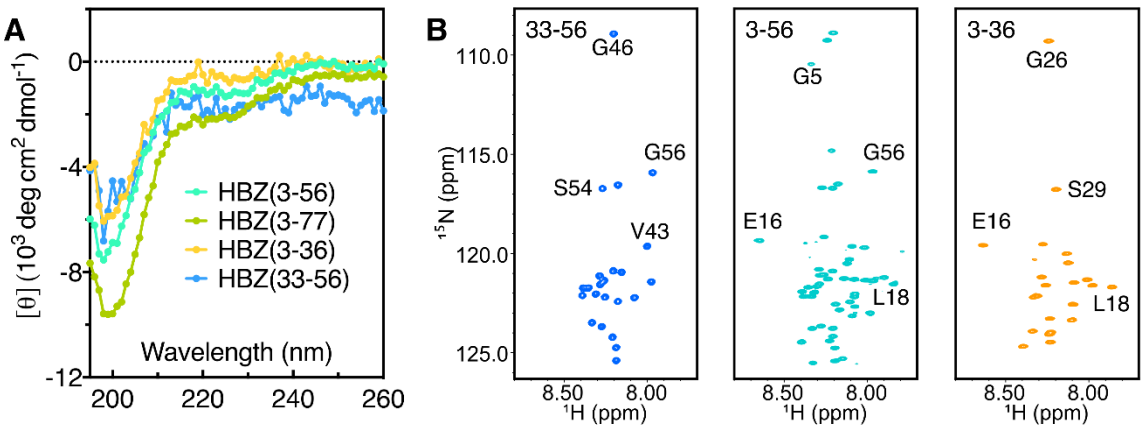

Fig. S1. (*A*) Far-UV CD spectra of HBZ AD constructs. (*B*) ^{1}H-^{15}N HSQC spectra of HBZ(33-56), HBZ(3-56) and HBZ(3-36) in their free forms, showing the lack of dispersion in the ^{1}H dimension (< 1 ppm) that indicates disorder.

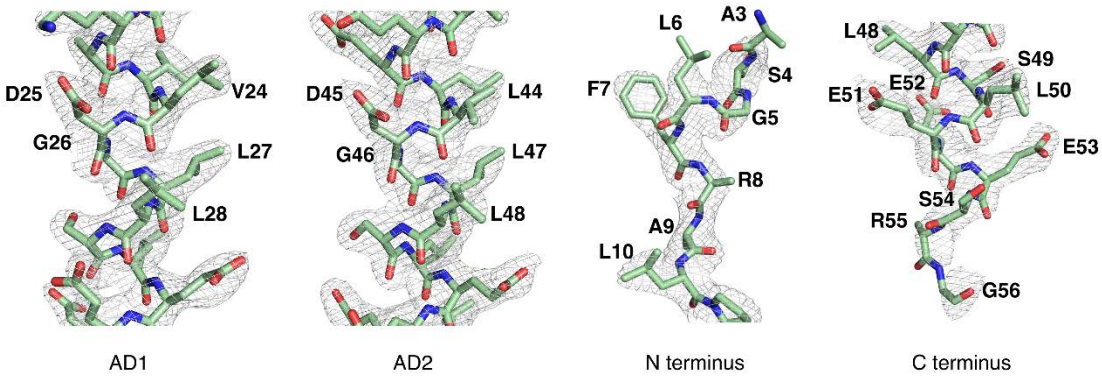

Fig. S2. Electron density (2Fo–Fc map) of the HBZ AD in the HBZ(3-77):KIX:c-Myb ternary complex.

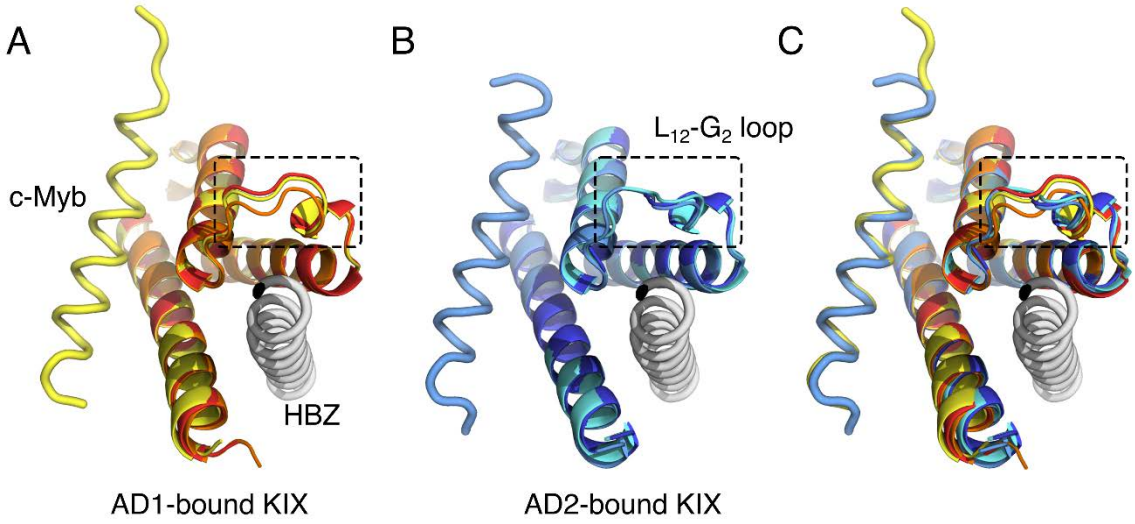

Fig. S3. Overlay of the six KIX structures in crystallographic asymmetric units of HBZ(3-77):KIX:c-Myb and HBZ(3-56):KIX:c-Myb reveal differences in the L_{12}-G_2 loop region between AD1-bound and AD2-bound KIX. *(A)* Overlay of 3 AD1-bound KIX structures. *(B)* Overlay of 3 AD2-bound KIX structures. (C) Overlay of all 6 KIX structures in the asymmetric units in the structures of the two ternary complexes.

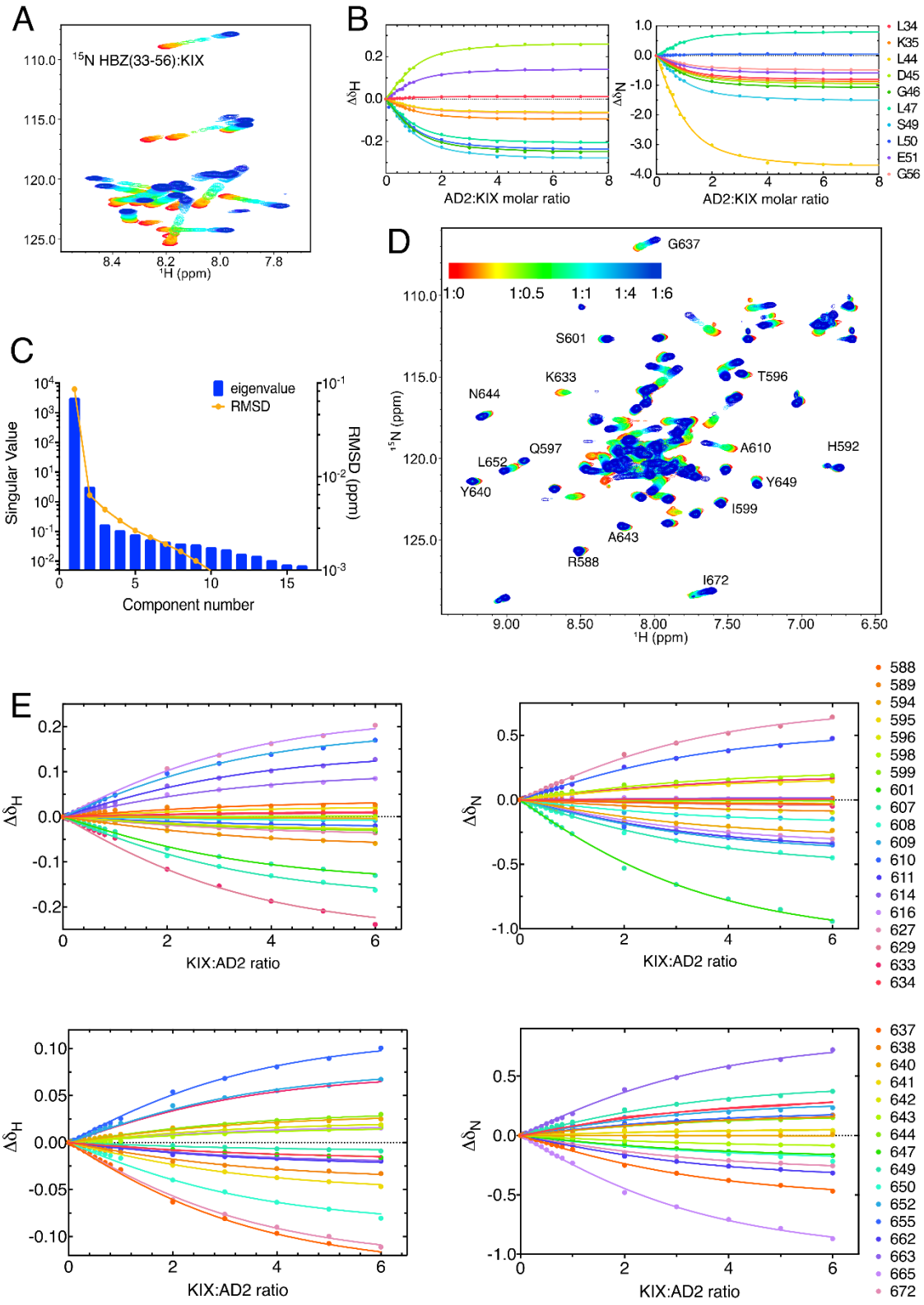
A
15N HBZ(33-56):KIX
1H (ppm)
B
AD2:KIX molar ratio
AD2:KIX molar ratio
L34
K35
L44
D45
G46
L47
S49
L50
E51
G56
C
eigenvalue
RMSD
Singular Value
RMSD (ppm)
Component number
D
G637
1:0
1:0.5
1:1
1:4
1:6
S601
K633
T596
N644
Q597
A610
H592
L652
Y649
Y640
I599
A643
R588
I672
15N (ppm)
1H (ppm)
E
KIX:AD2 ratio
KIX:AD2 ratio
KIX:AD2 ratio
KIX:AD2 ratio
588
589
594
595
596
598
599
601
607
608
609
610
611
614
616
627
629
633
634
637
638
640
641
642
643
644
647
649
650
652
655
662
663
665
672

Fig. S4. Residue-specific mapping of AD2:KIX interactions. *(A)* ^{1}H-^{15}N HSQC spectra overlay of ^{15}N-labeled HBZ(33-56) titrated with KIX showing chemical shift changes upon addition of KIX. *(B)* Titration curves for a subset of HBZ(33-56) resonances upon titration with KIX. The dots represent experimental chemical shift perturbations and the lines represent a global fitting using a one-site binding model. *(C)* Singular value decomposition (SVD) analysis of the ^{15}N-labeled KIX:AD2 titration to determine the number of binding sites on KIX involved in the interactions (1-site or 2-sites) obtained using our in-house software nmrKd (12). Blue bars show the singular values contributing to spectral changes in ^{15}N-labeled KIX upon titration sorted in decreasing order (logarithmic scale). Yellow dots show the rmsd (ppm) between the original data set and the reconstructed data set using the first i numbers of components. The first two components have significantly large singular values, indicating that two major species of KIX (free and bound) contribute to the titration. The spectral dataset reconstructed using only the first two components has a very small rmsd value of 0.006 ppm compared to the raw dataset, confirming one site binding as there are two major component contributing to the spectral changes during titration (free and bound form with only one site of KIX participating in the interaction). *(D)* ^{1}H-^{15}N HSQC spectra overlay of ^{15}N-labeled KIX titrated with HBZ(33-56) showing chemical shift changes upon addition of HBZ(33-56). *(E)* Titration curves for a subset of KIX resonances upon titration with HBZ(33-56). The dots represent experimental chemical shift perturbations and the lines represent a global fitting using a one-site binding model.

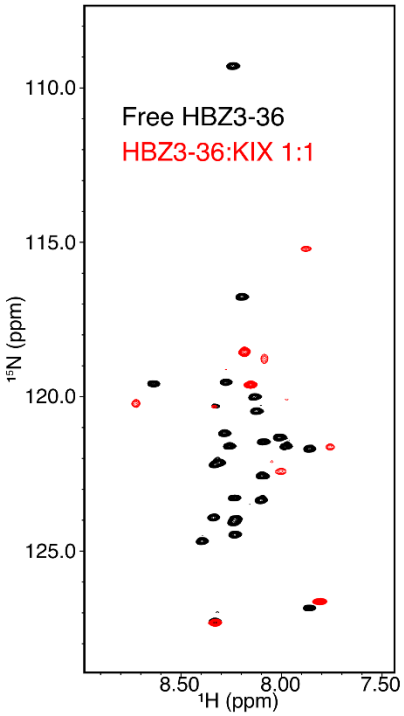

Fig. S5. Overlay of the ^{1}H-^{15}N HSQC spectra of free HBZ(3-36) (black) and HBZ(3-36):KIX 1:1 (red). Broadening of the resonances of HBZ(3-36) upon addition of KIX is shown by the absence of many of the red cross peaks.

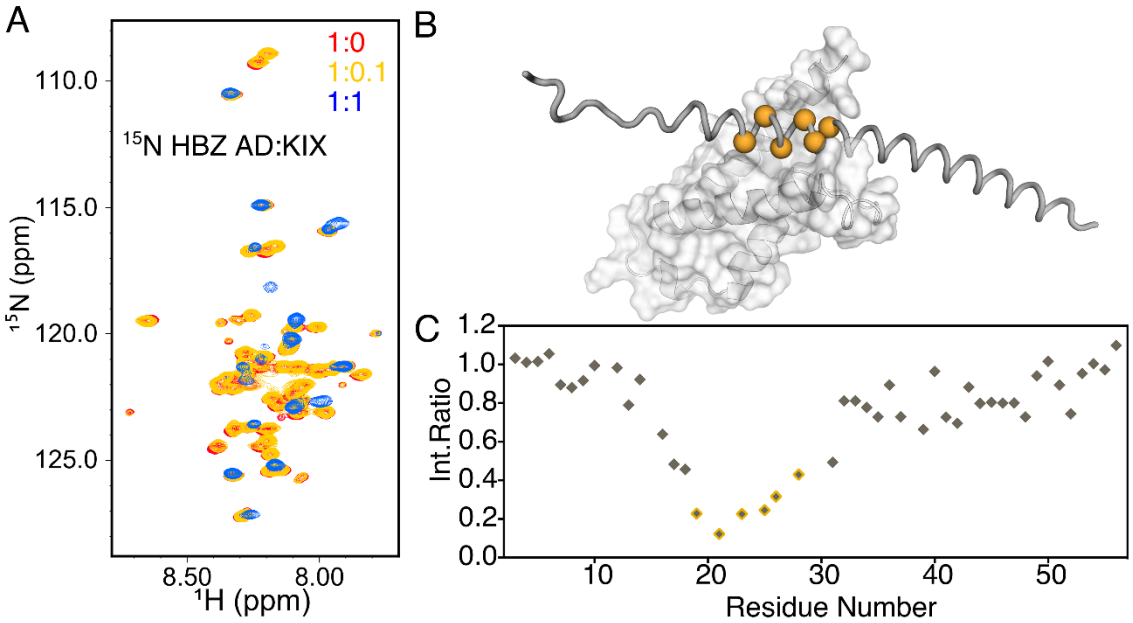

Fig. S6. AD1 as the predominant binding motif to KIX. *(A)* ^{1}H-^{15}N HSQC spectra overlay of free ^{15}N-labeled HBZ(3-56) (red), ^{15}N HBZ3-56 with 0.1x molar ratio of unlabeled KIX (yellow), and ^{15}N HBZ(3-56) with an equimolar amount of KIX (blue). Cross peaks of ^{15}N HBZ(3-56) severely broaden upon the addition of increased amount of KIX. (*B*) Residues of HBZ(3-56) with the most extensive intensity decrease upon addition of 0.1x KIX mapped onto the structure of HBZ AD as yellow spheres. (*C*) Histogram of peak intensity ratio in the ^{1}H-^{15}N HSQC spectra of HBZ(3-56) in the presence and absence of 0.1x molar concentration of KIX, i.e. the peak intensity ratio between the yellow and red spectra in (*A*). Residues with the most significant broadening are located in the AD1 region and highlighted in yellow.

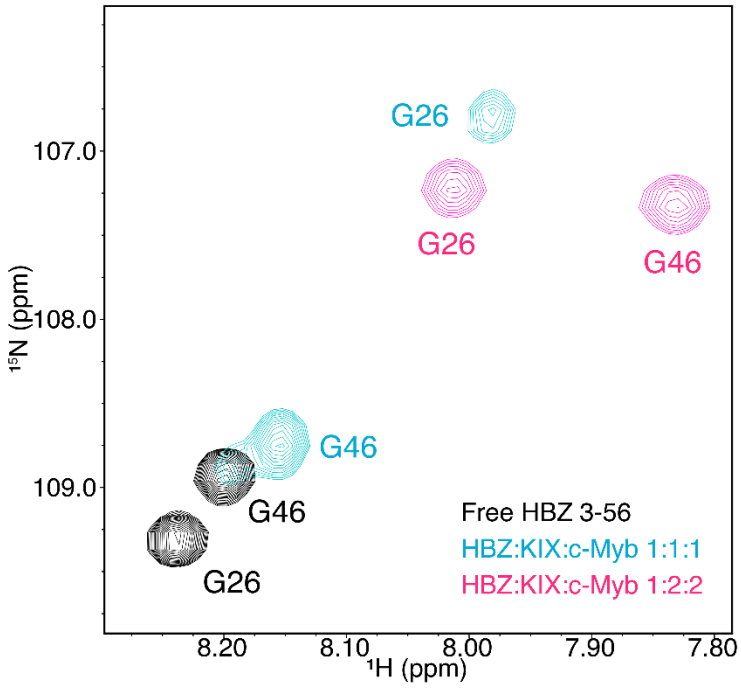

Fig. S7. Stoichiometry of the ternary complex HBZ AD:KIX:c-Myb shown by NMR. Overlay of a part of the ^{1}H-^{15}N HSQC spectra of ^{15}N labeled HBZ(3-56) in its free form (black), in complex with KIX and c-Myb in 1:1:1 molar ratio (cyan), and in complex with KIX and c-Myb in 1:2:2 molar ratio (pink).

HBZ(3-77)
into
KIX:c-Myb 1:1

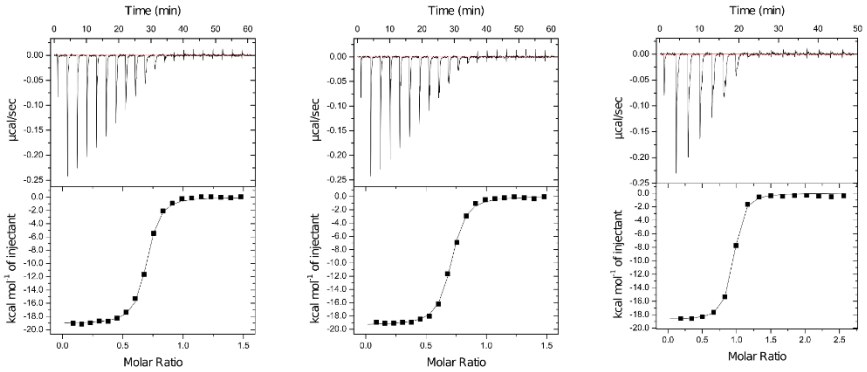

HBZ(3-77)
into KIX

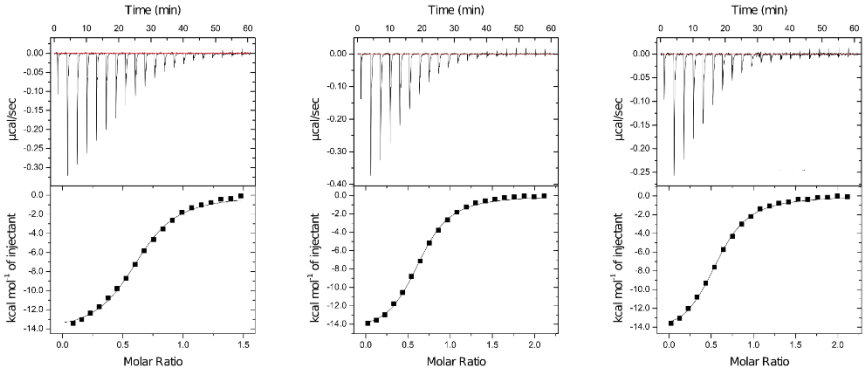

HBZ(3-56)
into
KIX:c-Myb 1:1

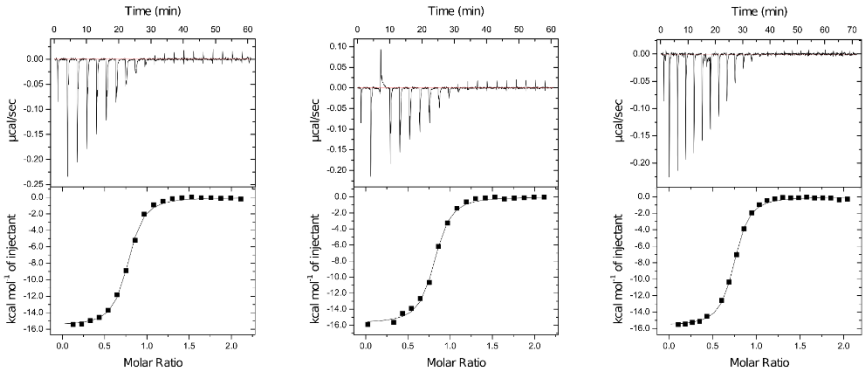

HBZ(3-56)
into KIX

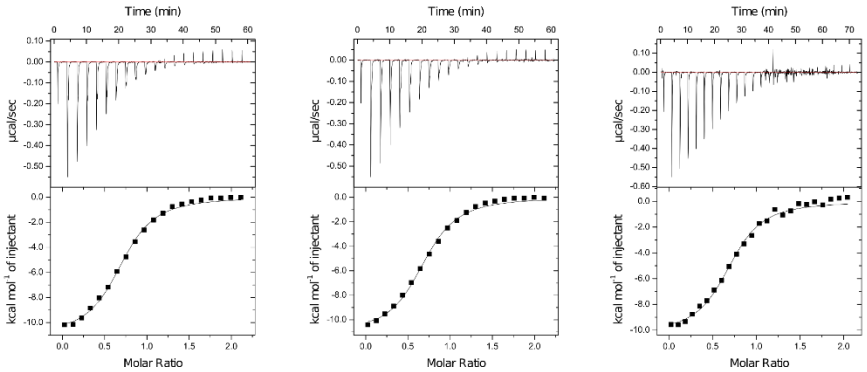

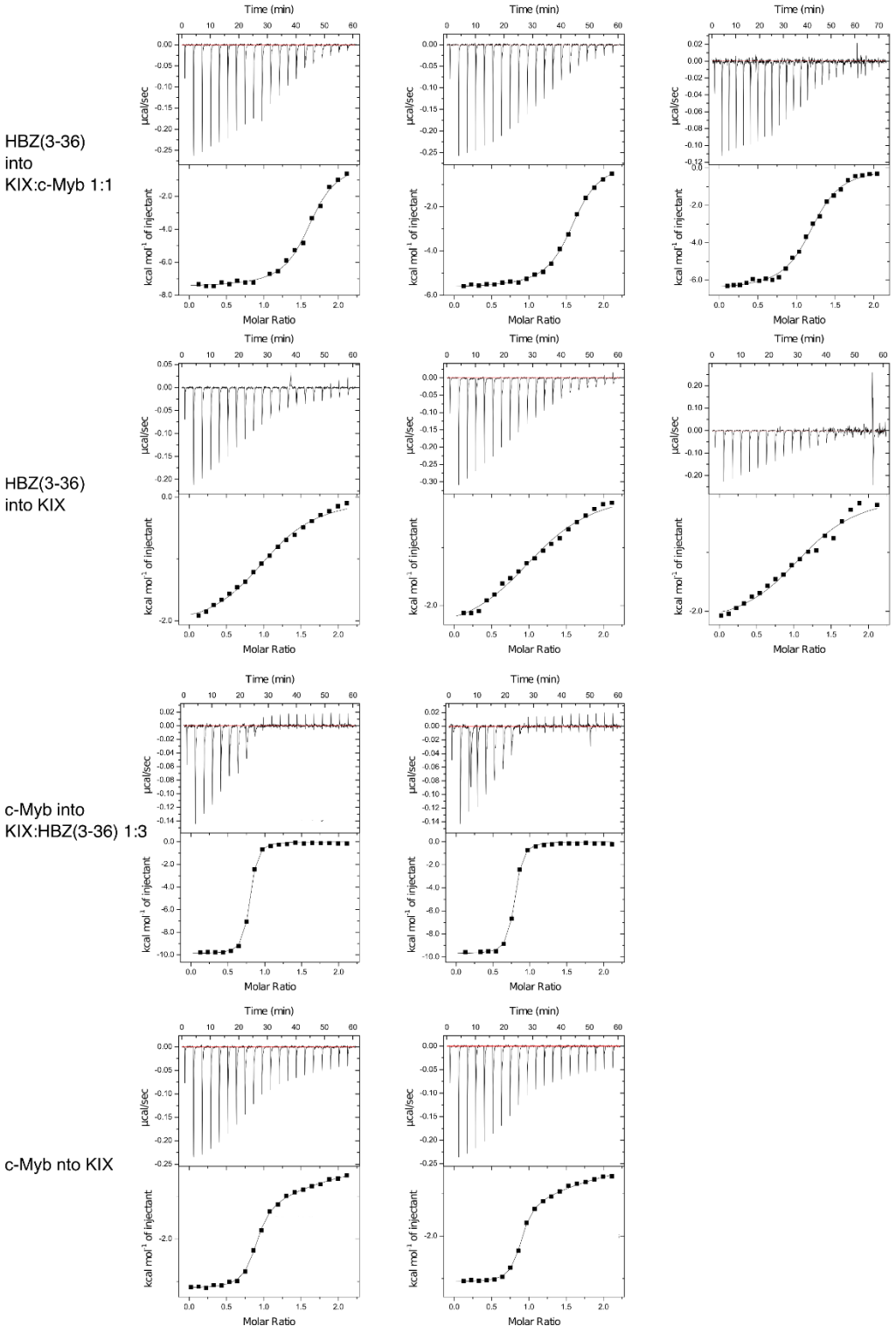

Fig. S8. ITC binding curves for HBZ, c-Myb and KIX forming binary and ternary complexes. Duplicate traces are shown in each horizontal line.

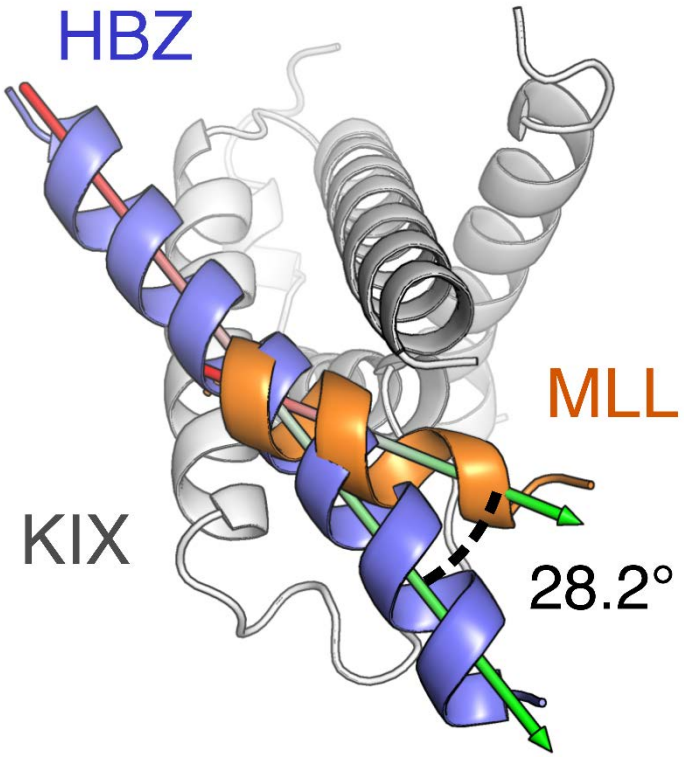

Fig. S9. HBZ and MLL bind to KIX in different orientations. HBZ (teal) and MLL (orange, PDB 2LXS) both bind in the same site on KIX (grey) but the orientations of their helix axes (dotted lines) relative to KIX are different.

Table S1. X-ray data collection and refinement statistics for KIX:c-Myb:HBZ complexes.

	KIX:c-Myb:HBZ(3-77)	KIX:c-Myb:HBZ(3-56)
Beamline	SSRL 9-2	SSRL 9-2
Wavelength (Å)	0.9795	0.9795
Resolution (Å)	50.00-2.35 (2.39-2.35)	50.00-2.80 (2.90-2.80)
Space group	C2	$P2_1$
Unit cell (Å, °)	a=118.83, b=51.17, c=72.05	a=55.00, b=80.31, c=64.64
	β = 126.4	β = 92.6
Total reflections[a]	64,072 (2,574)	79,559 (3,466)
Unique reflections	14,320 (660)	13,196 (642)
Redundancy	4.5 (3.9)	6.0 (5.4)
Completeness (%)	97.1 (88.9)	95.2 (90.6)
<I>/<σI>	13.7 (1.6)	16.6 (1.2)
R_{merge} (%)[b]	11.8 (82.8)	9.6 (>100)
R_{meas} (%)[c]	13.4 (95.4)	10.5 (>100)
R_{pim} (%)[d]	6.1 (45.9)	4.2 (53.6)
$CC_{1/2}$ (%)[e]	86.9 (56.2)	83.6 (34.4)
Refinement statistics		
Resolution (Å)	36.02-2.35	40.97-2.80
R_{work}/R_{free} (%)	19.9/22.9	23.9/30.1
Number of reflections in refinement (work/free)	13,686/628	11,861/660
Number of non-H protein atoms	2302	4187
Number of water molecules	34	0
Number of protein residues	278	489
RMS (bonds)	0.004	0.010
RMS (angles)	0.72	1.06
Ramachandran: favored, outliers (%)(13)	98.1, 0.0	98.4, 0.4
Clashscore[f]	4.0	5.0
Wilson B ($Å^2$)	38	94
Average B ($Å^2$)	59	98
Protein		
KIX	60	97
HBZ	63	103
c-Myb	72	97
Solvent	51	N/A

[a]Numbers in parentheses are for highest resolution shell
[b]$R_{merge} = \Sigma_{hkl} \Sigma_{i=1,n} |I_i(hkl) - \langle I(hkl) \rangle| / \Sigma_{hkl} \Sigma_{i=1,n} I_i(hkl)$
[c]$R_{meas} = \Sigma_{hkl} \sqrt{(n/n-1)} \Sigma_{i=1,n} |I_i(hkl) - \langle I(hkl) \rangle| / \Sigma_{hkl} \Sigma_{i=1,n} I_i(hkl)$
[d]$R_{pim} = \Sigma_{hkl} \sqrt{(1/n-1)} \Sigma_{i=1,n} |I_i(hkl) - \langle I(hkl) \rangle| / \Sigma_{hkl} \Sigma_{i=1,n} I_i(hkl)$
[e]$CC_{1/2}$ = Pearson Correlation Coefficient between two random half datasets
[f] Number of unfavorable all-atom steric overlaps ≥ 0.4Å per 1000 atoms

SI References

1. Sugase K, Dyson HJ, & Wright PE (2007) Mechanism of coupled folding and binding of an intrinsically disordered protein. *Nature* 447:1021-1025.
2. Otwinowski Z & Minor W (1997) Processing of X-ray diffraction data collected in oscillation mode. *Methods Enzymol* 276:307-326.
3. McCoy AJ, *et al.* (2007) Phaser crystallographic software. *J Appl Crystallogr* 40:658-674.
4. De Guzman RN, Goto NK, Dyson HJ, & Wright PE (2006) Structural basis for cooperative transcription factor binding to the CBP coactivator. *J. Mol. Biol.* 355:1005-1013.
5. Terwilliger TC, *et al.* (2013) Model morphing and sequence assignment after molecular replacement. *Acta Crystallogr. D Biol. Crystallogr.* 69:2244-2250.
6. Emsley P, Lohkamp B, Scott WG, & Cowtan K (2010) Features and development of Coot. *Acta Crystallogr D Biol Crystallogr* 66:486-501.
7. Adams PD, *et al.* (2010) PHENIX: a comprehensive Python-based system for macromolecular structure solution. *Acta Crystallogr D Biol Crystallogr* 66:213-221.
8. Murshudov GN, Vagin AA, & Dodson EJ (1997) Refinement of macromolecular structures by the maximum-likelihood method. *Acta Crystallographica Section D* 53:240-255.
9. Schrödinger L (2017) The PyMOL molecular graphics system, version 2.
10. Delaglio F, *et al.* (1995) NMRPipe: a multidimensional spectral processing system based on UNIX pipes. *J. Biomol. NMR* 6:277-293.
11. Johnson BA & Blevins RA (1994) Nmr View - a Computer-Program for the Visualization and Analysis of Nmr Data. *J. Biomol. NMR* 4:603-614.
12. Arai M, Ferreon JC, & Wright PE (2012) Quantitative analysis of multisite protein-ligand interactions by NMR: binding of intrinsically disordered p53 transactivation subdomains with the TAZ2 domain of CBP. *J. Am. Chem. Soc.* 134:3792-3803.
13. Chen VB, *et al.* (2010) MolProbity: all-atom structure validation for macromolecular crystallography. *Acta Crystallogr. D Biol. Crystallogr.* 66:12-21.